AIP ADVANCES **5**, 047150 (2015)

Impact of the cation-stoichiometry on the resistive switching and data retention of $SrTiO_3$ thin films

N. Raab,[a] C. Bäumer, and R. Dittmann
Peter Grünberg Institute and JARA-FIT, FZ Jülich, D-52425 Jülich, Germany

(Received 11 March 2015; accepted 21 April 2015; published online 29 April 2015)

Resistive switching oxides are investigated at great length as promising candidates for the next generation of non-volatile memories. It is generally assumed that defects have a strong impact on the resistive switching properties of transition metal oxides. However, the correlation between different types of defect structures and the switching properties is still elusive. We deposited single-crystalline $SrTiO_3$ thin films with various cation stoichiometry by pulsed laser deposition to investigate the stoichiometry related and therefore defect dependent influence on the resistive switching properties. This letter will reveal the differences in initial states, forming steps, switching characteristics as well as retention times taking into account both point defects and extended defects. We then propose an explanation on the basis of oxygen vacancy generation and redistribution to elucidate the dependence of the resistive switching properties on the cation stoichiometry dependent defect structure. © *2015 Author(s). All article content, except where otherwise noted, is licensed under a Creative Commons Attribution 3.0 Unported License.* [http://dx.doi.org/10.1063/1.4919697]

Resistive switching oxides are a promising candidate for future non-volatile memories.[1,2] The transition metal oxide $SrTiO_3$ is a model material for resistive switching oxides. Among various proposed resistive switching models, the filamentary switching based on oxygen migration is widely accepted for $SrTiO_3$.[3–5] In this framework of the filamentary switching, it is assumed that defects have a strong impact on the resistive switching properties.[6,7] Therefore a detailed knowledge of the thin film defect structure is mandatory to understand the observable resistive switching behavior.

The most important point defects in $SrTiO_3$ are vacancies, since interstitials are energetically not favorable in a perovskite structure.[8] For $SrTiO_3$ thin films with perfect cation stoichiometry only intrinsic background impurities and oxygen vacancies are present. Slight deviations from the perfect cation stoichiometry lead to the formation of cation vacancies to accommodate the cation-excess.[9] As a higher non-stoichiometry cannot be compensated solely by cation vacancies, different types of extended defects arise during growth, dependent on the cation stoichiometry: For Sr-excess thin films, e.g. Ruddlesden-Popper phases and antiphase-boundaries have been reported.[10–12] For Ti-excess thin films, e.g. amorphous TiO_2-inclusions and Sr-vacancy clusters have been reported.[10,13,14] By varying the growth parameters, $SrTiO_3$ thin films with different cation-stoichiometry and thus different types of defects can be created.

Regarding the switching properties, oxygen vacancy migration is widely accepted to explain the general resistive switching in $SrTiO_3$ thin films, but it is not sufficient to explain high retention times and fast switching simultaneously.[15] Therefore, extended defects have to be taken into account to combine both general resistive switching mechanism and individual device properties in $SrTiO_3$ thin films in a generalized model. Extended defects are indeed not mandatory for the resistive switching[16] but influence individual properties such as the filament forming step.[17,18] Therefore, the entire cation stoichiometry dependent defect structure of the respective thin films has to be considered.

[a]n.raab@fz-juelich.de

 ©Author(s) 2015

As this letter will show, varying the cation stoichiometry in $SrTiO_3$ thin films results in different initial states and different resistive switching properties, such as forming behavior and retention times. We then suggest a consistent explanation for the modified properties observed in non-stoichiometric thin films compared to thin films with nearly perfect cation stoichiometry.

We deposited 20 nm thick single-crystalline undoped $SrTiO_3$ thin films via pulsed laser deposition (PLD) on 0.5wt%-Nb:$SrTiO_3$ substrates (CrysTec). The single-crystalline $SrTiO_3$ target was ablated by a KrF excimer laser ($\lambda = 248$ nm) with a repetition rate of 5 Hz and a spot-size of 2 mm^2 at a target-to-substrate distance of 44 mm. To adjust the cation ratio in the thin films laser fluencies of 1.05, 1.50 and 2.25 Jcm^{-2} were used.[19] All samples were grown in an oxygen atmosphere of 0.1 mbar at a substrate temperature of 800° C and subsequently annealed for 10 minutes under unchanged conditions to ensure an oxidation equilibrium state. We characterized the thin films with X-ray Photoelectron Spectroscopy (XPS) and Atomic Force Microscopy (AFM). In both cases the transfer between the setups and the measurements were performed in ultra-high vacuum.

Figs. 1(a)-1(c) show the AFM topography images of the thin films grown with the different laser fluencies. The calculated root mean square roughness (RMS) as well as the Sr/Ti-ratio measured via XPS as a function of the laser fluence are presented in Fig. 1(d). The low laser fluence of 1.05 Jcm^{-2} results in a Sr-rich film (Sr/Ti = 1.11). Its surface consists of many islands on the step terraces, which we assume to be SrO islands. Single islands at the step edges are considerably higher than the average surface, resulting in a surface roughness of 0.6 nm. With medium laser fluence of 1.50 Jcm^{-2}, a stoichiometric thin film (Sr/Ti = 1.00) with a well-defined step terrace structure is obtained, which exhibits a surface roughness of 0.2 nm. The high laser fluence of 2.25 Jcm^{-2} results in a Ti-rich film (Sr/Ti = 0.94) with similar terrace structure but higher island density compared to the stoichiometric case, resulting in a slightly higher surface roughness of 0.3 nm. All three AFM images show surface structures that are characteristic for $SrTiO_3$ thin films with the particular cation stoichiometry.[20] After the thin film characterization, resistive switching

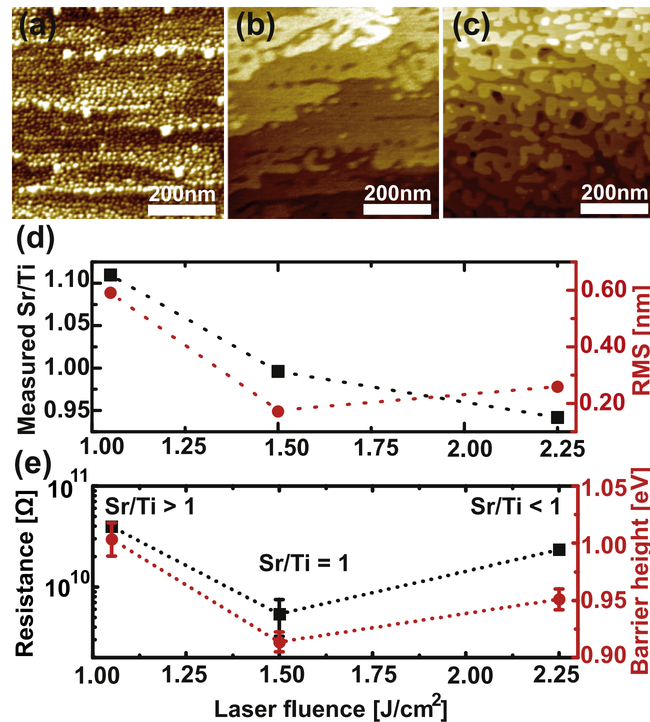

FIG. 1. (a)-(c) AFM topography of 20 nm thick homoepitaxial $SrTiO_3$ thin films with Sr/Ti = 1.11, Sr/Ti = 1.00 and Sr/Ti = 0.94, grown with a laser fluence of 1.05, 1.50 and 2.25 Jcm^{-2}, respectively. Step terraces are of unit cell height (~4 Å). (d) Sr-fraction (black squares) measured via XPS and topography roughness (red circles) calculated from the AFM images as well as (e) Schottky barrier height (black squares) and initial resistance (red circles) of the thin films as a function of the laser fluence.

metal-insulator-metal (MIM) devices were fabricated through evaporation of 30 nm platinum and patterning via standard photolithography and ion beam etching to obtain top electrodes with a size of 10 μm x 10 μm. All electrical measurements were performed with tungsten probes connected to a Keithley 2611A with the Nb:$SrTiO_3$ substrate acting as electrically grounded bottom electrode. The different sweeps were performed using the following voltage cycles: 0 V to +3 V for forming and SET, 0 V to -3 V for RESET and +0.5 V to -0.5 V for read-out. The device resistance was obtained from the slope of a linear fit of the read-out sweeps between -0.1 V and +0.1 V. The step size was 20 mV and the holding time before measurement was 5 ms; the current compliance for the forming step and the SET process was either 10 mA or 30 mA. During the RESET sweeps no current compliance was necessary.

First of all, read-out sweeps were performed to obtain the initial resistance, followed by a nominal RESET. Since the devices are initially in the high resistance state (HRS), no switching occurred; the resulting *I(V)*-curves correspond to the reverse direction of the initial Schottky barrier and were fitted to obtain the initial Schottky barrier height Φ_B.[21] Fig. 1(e) shows the initial state resistance (red circles) and the Schottky barrier height (black squares) as a function of the cation stoichiometry. Both properties were determined before forming and are averaged over at least nine devices to take the device to device variation into account. The stoichiometric film exhibits the lowest initial state resistance and Schottky barrier height, followed by the Ti-rich film and finally the Sr-rich film. Since the three samples have identical top-electrodes the differences in initial state resistance and Schottky barrier height only depend on the amount of electrons in the conduction band of the $SrTiO_3$ thin film. In non-stoichiometric films cation vacancies are generated to compensate the differing cation ratio.[9] Those cation vacancies are deep acceptors and are therefore lowering the amount of electrons contributing to the electrical transport. As a result of this lowering of effective charge carriers, the Schottky barrier height and consequently the initial state resistance is higher for non-stoichiometric films. The quantitative difference between the Sr-rich and the Ti-rich film originates from the different amount of cation vacancies present in the thin films.

The necessary forming step was performed with either 10 mA or 30 mA current compliance, which was kept constant during the subsequent measurements on each particular device. After the forming step, each device was switched between the low resistive state (LRS) and the high resistive state (HRS) and subsequently read-out several times to test the reproducibility of the resistive switching.

Fig. 2 shows forming steps (dashed lines) and subsequent SET curves (full lines) after a RESET (not shown) for different cation stoichiometries measured with a current compliance of 10 mA (a) and 30 mA (b), respectively. All devices exhibit a reproducible switching with a noticeable forming step. The superimposed curves in the LRS (upper branch) prove that the LRS after the forming step is the same as the LRS after the subsequent SET.

In good agreement with the lowest initial state resistance and Schottky barrier height (see Fig. 1(e)), the I(V)-slope of the stoichiometric film shows a steeper rise starting at a lower voltage compared to the non-stoichiometric films. The initial state difference between the Sr-rich and the Ti-rich is also reproduced in the forming step *I(V)*-curve, as the rise starts at ~1 V for the Sr-rich and at a lower voltage of ~0.6 V for the Ti-rich device. For higher voltages during the forming step, the current in the stoichiometric device increases continuously to the current compliance, whereas the current in the non-stoichiometric devices jumps abruptly to the current compliance. This jump denotes an abrupt increase of the conductivity for both non-stoichiometric films. Again quantitative differences between the Sr-rich and Ti-rich devices are observed, as the jump is more pronounced for the Sr-rich device.

In analogy to the forming step a voltage sweep from 0 V to +3 V sets the devices in a defined and reproducible LRS. For the non-stoichiometric devices, the hysteresis is more pronounced in comparison with the stoichiometric device. This results in a lower resistance for the LRS for non-stoichiometric devices, independent of the current compliance. However, for stoichiometric devices the *I(V)*-behavior undergoes two major changes with varying the current compliance. The first difference is the about two orders of magnitude lower resistance in the LRS for 30 mA current compliance at zero voltage. The second difference is the shape of the hysteresis, as it gets flatter for higher voltages at 30 mA current compliance, indicating a current saturation. All three films

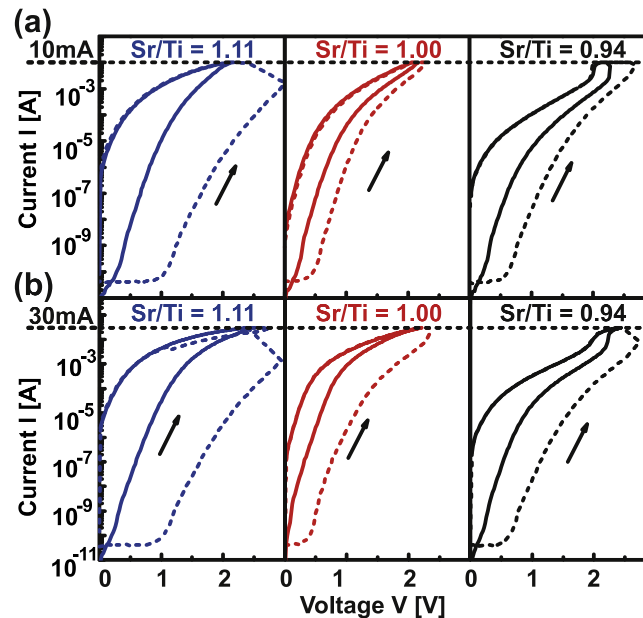

FIG. 2. Superimposed *I(V)*-curves of forming (dashed line) and SET (full line) with 10 mA (a) and 30 mA (b) current compliance for Sr/Ti = 1.11 (blue), Sr/Ti = 1.00 (red) and Sr/Ti < 0.94 (black). The arrow marks the switching polarity and the horizontal dashed line indicates the current compliance.

exhibit a reproducible resistive switching with the same polarity at both, 10 mA and 30 mA current compliance indicating the same general switching mechanism. As there are significant differences between stoichiometric and non-stoichiometric devices, however, the individual device properties are influenced by the cation stoichiometry dependent defect structure, as was mentioned in the introduction and will be discussed later.

The defect structure also has a very strong impact on the retention times of the resistance states. The retention was characterized for both resistance states (LRS and HRS) for each stoichiometry through read-out sweeps at fixed time intervals after switching. Fig. 3 shows characteristic retention data of the LRS (dashed lines) and HRS (full lines) for Sr-rich (a), stoichiometric (b) and Ti-rich (c) devices with a current compliance of 10 mA (black) and 30 mA (red), respectively. It is important to note that the LRS and HRS for a given current compliance were measured on the same device to accurately compare the resistance states.

All measured high resistive states are lower than the corresponding initial state resistances (see Fig. 1(e)) and show no tendency to shift towards the initial state within the first 300 hours. The HRS of the stoichiometric device at 30 mA current compliance exhibits the lowest resistance value and is the only HRS below 100 MΩ, therefore significantly reducing the memory window. Despite the initial resistance decrease, this HRS is also stable for at least 300 hours.

The low resistance states, however, show a significant difference in the retention between stoichiometric and non-stoichiometric films. In the stoichiometric film (b) the LRS measured directly after the SET is almost two orders of magnitude higher for 10 mA than for 30 mA current compliance. For 10 mA current compliance the LRS decays to the corresponding stable HRS in less than 150 hours, whereas for 30 mA current compliance the LRS is stable for at least 300 hours after an initial increase within 25 hours. Obviously the current compliance has a significant influence on both the initial LRS values and the LRS development over time for the stoichiometric device.

In the case of the Sr-rich (a) and Ti-rich (c) devices the low resistance states at 10 mA and 30 mA current compliance show a very similar behavior. After an increase of roughly one order of magnitude within 30 hours after the SET, all resistance states except the Ti-rich one with 30 mA current compliance are very stable over at least 300 hours. Despite the resistance increase of about one order of magnitude in this exceptional case, the device is still in a distinct LRS after 300 hours. Similar to forming and SET characteristics there are significant differences between the

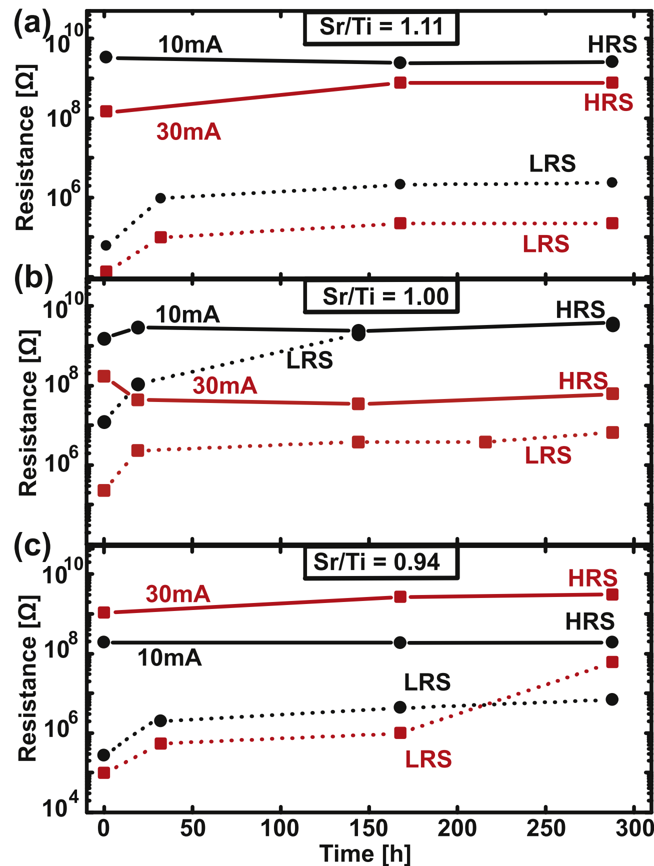

FIG. 3. Retention of the LRS (dashed line) and HRS (full line) over time for Sr/Ti > 1 (a), Sr/Ti = 1 (b) and Sr/Ti < 1 (c) with 10 mA (black circles) and 30 mA (red squares) current compliance, respectively. LRS and HRS were for all cases measured successively on the same device.

stoichiometric and the non-stoichiometric devices, that probably stem from the cation stoichiometry dependent defect structure.

Taking the different defect structures into account we suggest a consistent explanation for the observed differences between stoichiometric and non-stoichiometric devices. Fig. 4(a) schematically shows a stoichiometric device in the LRS with only oxygen vacancies (black circles) forming a filament. During the forming step the current and the Joule-heating induced local temperature becomes high enough to create such a filament through the generation and redistribution of oxygen vacancies.[22] By applying a sufficient RESET voltage the oxygen vacancies are detached from the electrode and the filament is interrupted. For the stoichiometric devices, the current compliance is

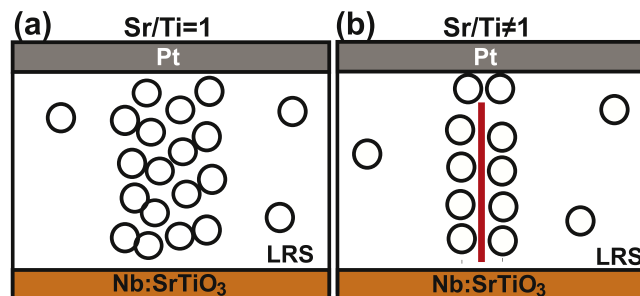

FIG. 4. (a) Filament in the LRS formed on the basis of only oxygen vacancies. (b) Filament in the LRS formed on the basis of an extend defect structure with pinned oxygen vacancies.

a crucial parameter, as it strongly influences the retention as well as the resistance values in LRS and HRS. A parameter to describe this observed current compliance influence consistently is the filament diameter.[23,24] For 10 mA the filament has a very small diameter, therefore it decomposes within a short time due to the lateral concentration gradient of oxygen vacancies in the vicinity of the filament. Due to the increased current and Joule-heating induced local temperature the filament for 30 mA has a larger diameter, which causes two effects: On the one hand the LRS retention time is much higher as the filament decomposes not completely within 300 hours. On the other hand the HRS is lowered as the applied negative voltage is not sufficient to fully interrupt the large filament. An additional effect may be a structural change in the local high temperature area through generation of additional defects, such as dislocations, which may alter the switching properties.[25]

While this explanation describes the observed behavior of the stoichiometric devices satisfactorily, it is not sufficient to describe the different behavior observed in the non-stoichiometric devices. As stated earlier the defect structure of the non-stoichiometric films contains cation vacancies, which lower the conductivity in the initial state. In the forming and SET characteristics, however, the conductivity in the LRS is increased for both non-stoichiometric devices. Therefore, the observed resistive switching behavior and retention are rather caused by additional extended defects present in the non-stoichiometric films. The presence of extended defects in our $SrTiO_3$ thin films has been shown in our earlier work.[9] For non-stoichiometric devices we consider extended defects as pre-defined but isolated current paths by pinning oxygen vacancies in their vicinity, resulting in an n-type conducting extended defect structure.[26–29] During the forming step, oxygen vacancy generation and redistribution leads to a connection of both electrodes through such an extended defect structure as filament core, as schematically depicted in Fig. 4(b). As soon as the extended defect is connected to both electrodes the pre-defined current path is activated, resulting in a current jump in the *I(V)*-curve (see Fig. 2). Quantitative differences in the current jumps between devices with different non-stoichiometry may originate from the different types and concentration of the extended defects providing the basis for the filament.

Regarding the retention times (see Fig. 3) the filaments in both non-stoichiometric devices, especially in the Sr-rich case, are very stable as the filaments are inhibited from decomposing through the pinning of oxygen vacancies at the extended defects.[27] As the extended defect filament is presumably thinner than a pure oxygen-deficient filament created at the same current compliance, the filament interruption during RESET is eased, resulting in a stable and distinct HRS with increased resistance compared to the stoichiometric device at 30 mA.

In conclusion, we have revealed the differences in the initial state properties, forming step, SET characteristics as well as LRS and HRS retention of single-crystalline $SrTiO_3$ thin films with different cation stoichiometry. We explain how the stoichiometry-induced defect structure of the thin films can account for the observed differences by taking into account extended defects as filament cores in non-stoichiometric films. We demonstrate that those extended defects are not implicitly necessary for the resistive switching effect to occur but are absolutely mandatory for good data retention. Our findings on the single-crystalline model system might be one of the reasons for the stabilization of the resistive switching in poly-crystalline transition metal oxide thin films.

ACKNOWLEDGMENTS

The authors gratefully acknowledge funding from the DFG (German Science Foundation) within the collaborative research center SFB 917 ”Nanoswitches” and from the W2/W3 program of the Helmholtz association. We thank R. Waser, F. Gunkel and S. Menzel for helpful discussions.

1 R. Waser and M. Aono, Nature Materials **6**, 833 (2007).
2 E. Linn, R. Rosezin, C. Kuegeler, and R. Waser, Nature Materials **9**, 403 (2010).
3 D. S. Jeong, H. Schroeder, U. Breuer, and R. Waser, Journal of Applied Physics **104**, 123716 (2008).
4 M. Janousch, G. I. Meijer, U. Staub, B. Delley, S. F. Karg, and B. P. Andreasson, Advanced Materials **19**, 2232 (2007).
5 R. Dittmann, R. Muenstermann, I. Krug, D. Park, T. Menke, J. Mayer, A. Besmehn, F. Kronast, C. Schneider, and R. Waser, Proceedings of the IEEE **100**, 1979 (2012).
6 R. Muenstermann, T. Menke, R. Dittmann, S. Mi, C.-L. Jia, D. Park, and J. Mayer, Journal of Applied Physics **108**, 124504 (2010).
7 K. Shibuya, R. Dittmann, S. Mi, and R. Waser, Advanced Materials **22**, 411 (2010).

[8] D. M. Smyth, *The defect chemistry of metal oxides* (Oxford University Press, New York, 2000).
[9] D. J. Keeble, S. Wicklein, L. Jin, C. L. Jia, W. Egger, and R. Dittmann, Physical Review B **87**, 195409 (2013).
[10] T. Suzuki, Y. Nishi, and M. Fujimoto, Philosophical Magazine A **80**, 621 (2000).
[11] Y. Tokuda, S. Kobayashi, T. Ohnishi, T. Mizoguchi, N. Shibata, Y. Ikuhara, and T. Yamamoto, Applied Physics Letters **99**, 173109 (2011).
[12] T. Ohnishi, K. Shibuya, T. Yamamoto, and M. Lippmaa, Journal of Applied Physics **103**, 103703 (2008).
[13] Y. Tokuda, S. Kobayashi, T. Ohnishi, T. Mizoguchi, N. Shibata, Y. Ikuhara, and T. Yamamoto, Applied Physics Letters **99**, 033110 (2011).
[14] H. Du, C. Jia, J. Mayer, J. Barthel, C. Lenser, and R. Dittmann, (2015).
[15] W. Jiang, M. Noman, Y. M. Lu, J. A. Bain, P. A. Salvador, and M. Skowronski, Journal of Applied Physics **110**, 034509 (2011).
[16] R. J. Kamaladasa, M. Noman, W. Chen, P. A. Salvador, J. A. Bain, M. Skowronski, and Y. N. Picard, Journal of Applied Physics **113**, 234510 (2013).
[17] C. Lenser, Z. Connell, A. Kovcs, R. Dunin-Borkowski, A. Koehl, R. Waser, and R. Dittmann, Applied Physics Letters **102**, 183504 (2013).
[18] Y. S. Kim, J. Kim, M. J. Yoon, C. H. Sohn, S. B. Lee, D. Lee, B. C. Jeon, H. K. Yoo, T. W. Noh, A. Bostwick, E. Rotenberg, J. Yu, S. D. Bu, and B. S. Mun, Applied Physics Letters **104**, 013501 (2014).
[19] S. Wicklein, A. Sambri, S. Amoruso, X. Wang, R. Bruzzese, A. Koehl, and R. Dittmann, Applied Physics Letters **101**, 131601 (2012).
[20] C. Xu, S. Wicklein, A. Sambri, S. Amoruso, M. Moors, and R. Dittmann, Journal of Physics D: Applied Physics **47**, 034009 (2014).
[21] S. M. Sze and K. K. Ng, *Physics of Semiconductor Devices* (John Wiley & Sons, 2006).
[22] S. Menzel, M. Waters, A. Marchewka, U. Boettger, R. Dittmann, and R. Waser, Advanced Functional Materials **21**, 4487 (2011).
[23] D. Ielmini, F. Nardi, and C. Cagli, Nanotechnology **22**, 254022 (2011).
[24] G. Bersuker, D. C. Gilmer, D. Veksler, P. Kirsch, L. Vandelli, A. Padovani, L. Larcher, K. McKenna, A. Shluger, V. Iglesias, M. Porti, and M. Nafra, Journal of Applied Physics **110**, 124518 (2011).
[25] W. Jiang, R. J. Kamaladasa, Y. M. Lu, A. Vicari, R. Berechman, P. A. Salvador, J. A. Bain, Y. N. Picard, and M. Skowronski, Journal of Applied Physics **110**, 054514 (2011).
[26] V. Metlenko, A. H. H. Ramadan, F. Gunkel, H. Du, H. Schraknepper, S. Hoffmann-Eifert, R. Dittmann, R. Waser, and R. A. D. Souza, Nanoscale **6**, 12864 (2014).
[27] M. Schie, A. Marchewka, T. Mueller, R. A. D. Souza, and R. Waser, Journal of Physics: Condensed Matter **24**, 485002 (2012).
[28] Z. Zhang, W. Sigle, W. Kurtz, and M. Ruehle, Physical Review B **66**, 214112 (2002).
[29] H. Du, C.-L. Jia, L. Houben, V. Metlenko, R. A. De Souza, R. Waser, and J. Mayer, Acta Materialia **89**, 344 (2015).